Competing interests None.

Provenance and peer review Not commissioned; externally peer reviewed.

REFERENCES

1. **Bachem MG,** Schneider E, Gross H, *et al*. Identification, culture, and characterization of pancreatic stellate cells in rats and humans. *Gastroenterology* 1998;**115**:421–32.
2. **Schneider E,** Schmid-Kotsas A, Zhao J, *et al*. Identification of mediators stimulating proliferation and matrix synthesis of rat pancreatic stellate cells. *Am J Physiol Cell Physiol* 2001;**281**:C532–43.
3. **Shimizu K,** Shiratori K, Kobayashi M, *et al*. Troglitazone inhibits the progression of chronic pancreatitis and the profibrogenic activity of pancreatic stellate cells via a PPARgamma-independent mechanism. *Pancreas* 2004;**29**:67–74.
4. **Yamada T,** Kuno A, Masuda K, *et al*. Candesartan, an angiotensin II receptor antagonist, suppresses pancreatic inflammation and fibrosis in rats. *J Pharmacol Exp Ther* 2003;**307**:17–23.
5. **Kuno A,** Yamada T, Masuda K, *et al*. Angiotensin-converting enzyme inhibitor attenuates pancreatic inflammation and fibrosis in male Wistar Bonn/Kobori rats. *Gastroenterology* 2003;**124**:1010–19.
6. **Sato Y,** Murase K, Kato J, *et al*. Resolution of liver cirrhosis using vitamin A-coupled liposomes to deliver siRNA against a collagen-specific chaperone. *Nat Biotechnol* 2008;**26**:431–42.
7. **Buchholz M,** Kestler HA, Holzmann K, *et al*. Transcriptome analysis of human hepatic and pancreatic stellate cells: organ-specific variations of a common transcriptional phenotype. *J Mol Med* 2005;**83**:795–805.
8. **Apte MV,** Haber PS, Applegate TL, *et al*. Periacinar stellate shaped cells in rat pancreas: identification, isolation, and culture. *Gut* 1998;**43**:128–33.
9. **Williams EJ,** Benyon RC, Trim N, *et al*. Relaxin inhibits effective collagen deposition by cultured hepatic stellate cells and decreases rat liver fibrosis in vivo. *Gut* 2001;**49**:577–83.
10. **Inoue M,** Ino Y, Gibo J, *et al*. The role of monocyte chemoattractant protein-1 in experimental chronic pancreatitis model induced by dibutyltin dichloride in rats. *Pancreas* 2002;**25**:e64–70.
11. **Merkord J,** Jonas L, Weber H, *et al*. Acute interstitial pancreatitis in rats induced by dibutyltin dichloride (DBTC): pathogenesis and natural course of lesions. *Pancreas* 1997;**15**:392–401.
12. **Elsasser HP,** Haake T, Grimmig M, *et al*. Repetitive cerulein-induced pancreatitis and pancreatic fibrosis in the rat. *Pancreas* 1992;**7**:385–90.
13. **Puig-Divi V,** Molero X, Salas A, *et al*. Induction of chronic pancreatic disease by trinitrobenzene sulfonic acid infusion into rat pancreatic ducts. *Pancreas* 1996;**13**:417–24.
14. **Merkord J,** Weber H, Jonas L, *et al*. Influence of ethanol on long-term effects of dibutyltin dichloride (DBTC) in pancreas and liver of rats. *Hum Exp Toxicol* 1998;**17**:144–50.
15. **Yamamoto M,** Otani M, Otsuki M. A new model of chronic pancreatitis in rats. *Am J Physiol Gastrointest Liver Physiol* 2006;**291**:G700–8.
16. **Tsuchitani M,** Saegusa T, Narama I, *et al*. A new diabetic strain of rat (WBN/Kob). *LabAnim* 1985;**19**:200–7.
17. **Sparmann G,** Merkord J, Jaschke A, *et al*. Pancreatic fibrosis in experimental pancreatitis induced by dibutyltin dichloride. *Gastroenterology* 1997;**112**:1664–72.
18. **Ishibashi T,** Zhao H, Kawabe K, *et al*. Blocking of monocyte chemoattractant protein-1 (MCP-1) activity attenuates the severity of acute pancreatitis in rats. *J Gastroenterol* 2008;**43**:79–85.
19. **Iredale JP,** Benyon RC, Pickering J, *et al*. Mechanisms of spontaneous resolution of rat liver fibrosis. Hepatic stellate cell apoptosis and reduced hepatic expression of metalloproteinase inhibitors. *J Clin Invest* 1998;**102**:538–49.
20. **Weidenbach H,** Lerch MM, Turi S, *et al*. Failure of a prolyl 4-hydroxylase inhibitor to alter extracellular matrix deposition during experimental pancreatitis. *Digestion* 1997;**58**:50–7.
21. **Masamune A,** Watanabe T, Kikuta K, *et al*. Roles of pancreatic stellate cells in pancreatic inflammation and fibrosis. *Clin Gastroenterol Hepatol* 2009;**7**:S48–54.
22. **Jain RK.** Normalizing tumor vasculature with anti-angiogenic therapy: a new paradigm for combination therapy. *Nat Med* 2001;**7**:987–9.
23. **Hideshima K,** Seike J, Mimura S, *et al*. HSP47 and angiogenic factor expression and its implication for the healing of periosteal defects in the mouse cranium. *Oral Med Pathol* 2006;**11**:27–33.
24. **Okada H,** Inoue T, Kanno Y, *et al*. Selective depletion of fibroblasts preserves morphology and the functional integrity of peritoneum in transgenic mice with peritoneal fibrosing syndrome. *Kidney Int* 2003;**64**:1722–32.
25. **Zhou X,** Hovell CJ, Pawley S, *et al*. Expression of matrix metalloproteinase-2 and -14 persists during early resolution of experimental liver fibrosis and might contribute to fibrolysis. *Liver Int* 2004;**24**:492–501.
26. **Steffensen B,** Wallon UM, Overall CM. Extracellular matrix binding properties of recombinant fibronectin type II-like modules of human 72-kDa gelatinase/type IV collagenase. High affinity binding to native type I collagen but not native type IV collagen. *J Biol Chem* 1995;**270**:11555–66.

Treatment of pancreatic fibrosis with siRNA against a collagen-specific chaperone in vitamin A-coupled liposomes

Hirotoshi Ishiwatari, Yasushi Sato, Kazuyuki Murase, et al.

Gut published online November 20, 2012
doi: 10.1136/gutjnl-2011-301746

Notes

The Prostate 73:500–511 (2013)

Zoledronic Acid But Not Somatostatin Analogs Exerts Anti-Tumor Effects in a Model of Murine Prostatic Neuroendocrine Carcinoma of the Development of Castration-Resistant Prostate Cancer

Kohei Hashimoto,[1] Naoya Masumori,[1]* Toshiaki Tanaka,[1] Toshihiro Maeda,[1] Ko Kobayashi,[1] Hiroshi Kitamura,[1] Koichi Hirata,[2] and Taiji Tsukamoto[1]

[1]Department of Urology, Sapporo Medical University School of Medicine, Japan
[2]First Department of Surgery, Sapporo Medical University School of Medicine, Japan

BACKGROUND. Since neuroendocrine (NE) cells play an important role in the development of castration-resistant prostate cancer (CRPC), target therapy to NE cells should be considered for treating CRPC. We investigated the effects zoledronic acid (ZOL) and two somatostatin analogs (octreotide: SMS, and pasireotide: SOM) on an NE allograft (NE-10) and its cell line (NE-CS), which were established from the prostate of the LPB-Tag 12T-10 transgenic mouse.

METHODS. We examined the in vivo effects of ZOL, SMS and SOM as single agents and their combinations on subcutaneously inoculated NE-10 allografts and the in vitro effects on NE-CS cells. Apoptosis and cell cycle activity were assessed by immunohistochemistry using TdT-mediated dUTP-biotin nick-end labeling (TUNEL) and a Ki-67 antibody, respectively.

RESULTS. In vivo growth of NE-10 tumors treated with ZOL, ZOL plus SMS, or ZOL plus SOM was significantly inhibited compared to the control as a consequence of induction of apoptosis and cell cycle arrest. ZOL induced time- and dose-dependent inhibition of in vitro proliferation of NE-CS cells, but the somatostatin analogs (SMS and SOM) did not. ZOL also inhibited migration of NE-CS cells. These effects were caused by inhibition of Erk1/2 phosphorylation via impairment of prenylation of Ras.

CONCLUSIONS. ZOL, but not SMS or SOM, induced apoptosis and inhibition of proliferation and migration through impaired prenylation of Ras in NE carcinoma models. Our findings support the possibility that ZOL could be used in the early phase for controlling NE cells, which may trigger progression to CRPC. *Prostate 73: 500–511, 2013.*

KEY WORDS: **zoledronic acid; somatostatin analog; neuroendocrine carcinoma; prostate cancer; anti-tumor effect**

INTRODUCTION

Prostate cancer is the most common non-cutaneus malignancy in men in developed countries [1]. Its incidence has been gradually increasing even in non-Caucasian men. As the growth of cancer cells is androgen-dependent, androgen deprivation therapy including surgical or chemical castration has been the mainstay of treatment for advanced prostate cancer. The response to this treatment lasts for a median of 36–48 months [2]. However, in most cases, the disease progresses despite the castration level of serum testosterone, and results in castration-resistant prostate cancer (CRPC). The prognosis of CRPC is poor and a concrete treatment strategy has not yet been established.

*Correspondence to: Naoya Masumori, Department of Urology, Sapporo Medical University School of Medicine S1, W16, Chuo-ku, Sapporo 060-8543, Japan. E-mail: masumori@sapmed.ac.jp
Received 4 June 2012; Accepted 27 August 2012
DOI 10.1002/pros.22590
Published online 19 September 2012 in Wiley Online Library (wileyonlinelibrary.com).

The exact mechanisms behind progression to castration resistance remain poorly understood. However, recent studies suggest that neuroendocrine (NE) cells, as well as pathways involving or bypassing the androgen receptor (AR), may play an important role in the development of castration resistance [3]. NE cells are present in both the normal and neoplastic prostate. They regulate surrounding prostate cells by secreting growth-modulating neuropeptides such as chromogranin A, serotonin and parathyroid hormone-related protein (PTHrP) [4]. Increases in the NE phenotype and secretory products are thought to be closely associated with progression and castration resistance in prostate cancer [5,6]. Previously, we developed an NE allograft (NE-10) and its cell line (NE-CS) from the prostate of the LPB-Tag 12T-10 transgenic mouse [7–9]. We demonstrated that secretions from NE cells induced androgen-independent growth of human prostate cancer cell line LNCaP and promoted pulmonary metastasis [10]. Therefore, it is crucial to seek a new drug or drug combinations targeting these prostatic NE carcinoma models (NE-10 and NE-CS).

Zoledronic acid (ZOL) is a nitrogen-containing bisphosphonate that inhibits bone resorption of osteoclasts through the inhibition of farnesyl-pyrophosphate synthetase in the mevalonate pathway. This agent has been demonstrated to have beneficial effects in patients with bone metastases of prostate cancer, reducing bone pain and skeletal-related events [11]. ZOL was also shown to have direct anti-tumor activity in several cancer cell lines. It is suggested that ZOL inhibits proliferation and induces apoptosis by impairment of prenylation of Ras and other small GTP-binding proteins (G proteins) [12].

Somatostatin is a peptide hormone that regulates secretion of various exocrine and endocrine glands via specific somatostatin receptors (SSTR). Five different subtypes (SSTR1-5), which are coupled to G proteins, have been identified [13]. Since a majority of NE tumors predominantly express SSTR2, somatostatin analogs having high affinity for SSTR2a such as octreotide (SMS) are considered to be drugs for NE tumors [14,15]. Since several studies have reported that SSTR1 and SSTR5 are expressed in addition to SSTR2 in prostate cancer tissue [15,16], new somatostatin analogs such as pasireotide (SOM) that have high affinity for SSTR5 in addition to SSTR2 [17], may be useful as new drugs for prostatic NE carcinoma.

In the present study, we investigated whether the growth of NE carcinoma models (NE-10, NE-CS) could be influenced by ZOL and/or somatostatin analogs (SMS and SOM), having potential anti-tumor activities.

MATERIALS AND METHODS

Cell Lines and Lell Culture

NE-CS is a murine prostate neuroendocrine cancer cell line established in our institute [9]. It was derived from an NE-10 tumor [8]. Passage numbers between 12, and 16 were used in the study. The NE-CS cells were maintained in the culture medium described below in 5% CO_2 in a humidified incubator. The medium consisted of RPMI-1640 (Gibco BRL, Breda, The Netherlands) that was supplemented with MEM nonessential amino acid (10 ml/L, Gibco BRL), MEM sodium pyruvate, penicillin–streptomycin (10 ml/L, Gibco BRL), 10% fetal bovine serum (FBS, ICN Biomedicals, Costa Mesa, CA), and 7.5% $NaHCO_3$.

ReverseTranscription Polymerase Chain Reaction (RT-PCR) Analysis

To investigate expression of SSTR in NE-10, RT-PCR analysis was performed. Tumor tissues in allografts of NE-10 were homogenized. Total RNA was extracted using an RNeasy kit (Qiagen, Valencia, CA) according to the manufacturer's instructions. A total of 2 μg of total RNA was reverse transcribed in a thermal cycles (Perkin–Elmer, Norwalk, CT) using SuperScript III (Invitrogen, Carlsbad, CA) and oligo (dT) 12–18 primers according to the manufacturer's instructions for 1 hr at 50°C in a 40 μl reaction mixture. Resulting cDNA (1 μl) was amplified with Taq polymerize and one set of oligonucleotide primers. Samples were denatured for 5 min at 94°C, and then amplified for 35 cycles at 94°C for 30 sec, 57°C for 30 sec, and 72°C for 1 min. Aliquots (9 μl) from each PCR sample were then analyzed by agarose-gel electrophoresis. Forward and reverse primer sequences were as follows: SSTR2a (5′-CAGCTGTACCATCAACTGGC, 5′-ATTTGTCCTGCTTACTGTCG), SSTR2b (5′-TGATCAATGTAGCTGTGTGG, 5′-CAAAGAACATTCTGGAAGC), SSTR5 (5′-TGCCTGATGGTCATGAGTGT, 5′-GGAAACTCTGGCGGAAGTTA), GAPDH (5′-TACAGCAACAGGGTGGTGGA, 5′-ACCACAGTCCATGCCATCAC).

Growth of NE-10 Allografts InVivo

To examine the in vivo effects of ZOL, SMS and SOM as single agents and their combinatorial effects on prostatic NE carcinoma, we used NE-10 allografts. Six-week-old male BALB/c nude mice were castrated using the scrotal approach. After one week, 50 mg tissue fragments of the NE-10 allograft were inoculated subcutaneously (s.c.) into the flanks of mice. Two weeks after transplantation, NE-10 tumors grew to a volume of more than 100 mm^3. The mice were then

randomized into six treatment groups (13 mice in each group): ZOL, SMS, SOM, ZOL plus SMS, ZOL plus SOM, and control. The groups were treated for 6 weeks with ZOL (1 μg/mouse, three times per week, s.c.), SMS (2 μg/mouse, once per day, s.c.), SOM (2 μg/mouse, twice per day, s.c.), ZOL plus SMS (1 μg/mouse, three times per week, s.c. plus 2 μg/mouse, once per day, s.c.), ZOL plus SOM (1 μg/mouse, three times per week, s.c. plus 2 μg/mouse, twice per day, s.c.), or saline (an equal volume of solvent/day, s.c.). These substances were dissolved in 100 μl saline. ZOL, SMS, and SOM were kindly provided by Novartis Pharma AG (Basel, Switzerland). These agents were soluble in saline. The body weights of mice were measured each week. The effects of treatments on tumor growth were determined by measuring tumor volume (0.523 × long diameter^2 × short diameter). After 6 weeks of treatment, the mice were killed and the tumor and liver were removed. Liver weight was measured, and the numbers of metastatic nodules on the liver surface were macroscopically counted. The tissues were fixed in 10% formalin and embedded in paraffin. The 5 μm thick paraffin-embedded material was routinely processed for hematoxylin and eosin staining.

The Animal Experiment Committee of Sapporo Medical University approved the in vivo experiments. Animal care and housing followed the guidelines of the Animal Experiment Committee.

Cell Cycle and Apoptosis Analysis of Tissue Sections

Immunohistochemical staining was done with formalin-fixed paraffin-embedded tissue sections of NE-10 tumors. The 5 μm thick sections were deparaffinized in xylene and rehydrated in graded alcohol. Antigen retrieval was done by boiling sections for 20 min in a microwave oven in preheated 0.01 mol/L sodium citrate buffer (pH 6.0). Endogenous peroxidase activity was blocked by 3% hydrogen peroxide in ethanol for 10 min. After blocking with 1% non-fat dry milk in phosphate-buffered saline (PBS) (pH 7.4), the sections were reacted with a rabbit polyclonal anti-Ki-67 antibody (Abcam plc., Cambridge, UK) at 20 μg/ml or preimmune sera for 1 hr, followed by incubation with biotinylated goat anti-rabbit IgG (Nichirei, Tokyo, Japan) for 30 min. Subsequently, the sections were stained with streptavidin-biotin complex (Nichirei), followed by incubation with 3,3-diaminobenzidine and counterstaining with hematoxylin. The same tissues were immunostained by TdT-mediated dUTP-biotin nick-end labeling (TUNEL) (In situ Apoptosis Detection Kit, Takara Bio, Inc., Otsu, Japan). The Ki-67 labeling index (KI) and apoptotic index (AI) were determined as the ratios of immunohistochemically positive cells per 1,000 NE cells by using a fluorescence microscope (model BZ-9000; Keyence, Osaka, Japan).

Proliferation Assays

NE-CS cells (1 × 104) were suspended with 100 μl of culture medium in a 96-well plate for 24 hr, and then treated with the indicated concentrations (from 0.1 to 100 μmol/L) of ZOL, SMS and SOM for 24, 48, or 72 hr. For combination, the same concentrations of ZOL and SMS or SOM were used; for example, 1 μmol/L of ZOL to 1 μmol/L of SMS. In addition, they were treated with the indicated concentrations (from 0.1 to 100 μmol/L) of ZOL plus 1, 5, and 20 μmol/L of farnesyl-pyrophosphate ammonium salt (FOH) (Sigma–Aldrich, St. Louis, MO) for 48 hr. FOH is an isoprenoid to be involved in prenylation of several G proteins including Ras in the intracellular mevalonate pathway. Cell proliferation was assessed using a WST-8 (modified tetrazolium salt) cell proliferation kit (Cell Counting Kit-8, Dojin, Japan). Changes in absorbance at 450 nm were measured with a microplate reader. The growth inhibition was determined as the concentration inducing 50% inhibition (IC50). For analysis of the synergism between ZOL and somatostatin analogs (SMS and SOM), the combination indices (CI) were calculated by the isobologram equation method [18,19], and CI values of <1, 1, and >1 were considered to indicate synergistic, additive, and antagonistic effects, respectively 12.

Cell Cycle and Apoptosis Assays

NE-CS cells (3 × 104) were suspended with 100 μl of culture medium in a 96-well plate for 24 hr, and then treated with various concentrations of ZOL (from 10 to 100 μmol/L) for 48 hr. Then the cells were fixed with 4% paraformaldehyde, permeabilized with 0.1% Triton X-100, and labeled with the TUNEL technique (In situ Cell Death Detection Kit TMR red, Roche Diagnostics, Mannheim, Germany) and the primary anti-Ki-67 antibody at a 1/200 dilution (Abcam plc., Cambridge, UK). The Ki-67 antibody was detected with an Alexa Fluor 488 donkey anti-rabbit antibody, and nuclei were stained with 4,6-diamidino-2-phenylindole (DAPI) (Invitrogen, Carlsbad, CA). As in the in vivo study, the KI and the AI were measured by fluorescence immunohistochemistry using a fluorescence microscope (model BZ-9000; Keyence, Osaka, Japan).

Migration Assays

Cell migration analyses were performed as described previously (10). In a trans-well culture

chamber (Coster Science, Cambridge, MA), a polyvinylpyrrolidone-free polycarbonate filter with an 8.0 μm pore size was precoated with 5 μg of fibronectin (Biomedical Technologies, Stoughton, MA) on the lower surface. Two different experiments were performed. In experiment 1, NE-CS cells (1×10^5) were placed in the upper chamber with 100 μl of culture medium with or without ZOL (10, 100 μmol/L). In the lower chamber, 600 μl of culture medium was added. In experiment 2, NE-CS cells (1×10^5) were placed in the upper chamber with 100 μl of culture medium adding 20 μmol/L of FOH with or without ZOL (10, 100 μmol/L). In the lower chamber, 600 μl of culture medium was added. The cells that migrated across the pores at 2, 4, 6, and 8 hr were counted under a microscope after hematoxylin and eosin staining. The experiments were carried out in triplicate. Data are shown as number of cells 1 mm^{-2} of membrane.

Pull Down and Western Blot Assays

NE-CS cells (1×10^5) were suspended with 2 ml of culture medium in a 6-well plate for 24 hr, and then treated with ZOL (10, 100 μmol/L) or ZOL (10, 100 μmol/L) + 20 μmol/L FOH for 48 hr. Subsequent to the treatment, cells were washed three times with ice-cold PBS and solubilized in lysis buffer [RIPA buffer, 100 mmol/L PMSF, 500 mmol/L Na_3VO_4, 1 mol/L NaF, 2 mol/L Sigma 104 phosphatase substrate, Protease Inhibitor Mini Cocktail]. The total protein content of the cell lysates was determined by the BCA Protein Assay (Pierce, Rockford, IL).

Activated Ras was detected by pull-down assay. The GTP-bound form of Ras in the cell lysates was affinity-purified using the Raf1-Ras-binding domain (RBD)-GST complexed with glutathione beads following the manufacturer's instructions (Active Ras Pull Down and Detection Kit, Thermo Fisher Science, Waltham, MA). Complexes were analyzed by SDS–PAGE and immunobloting with a Ras-specific antibody.

The cells lysates obtained were boiled in SDS sample buffer containing 0.5 mol/L 2-mercaptoethanol. Samples were separated by SDS–PAGE, transferred to polyvinylidene difluoride (PVDF) membranes and immunoblotted with rabbit monoclonal anti-Erk1/2 and anti-phospho-Erk1/2 antibodies (Cell Signaling Technology Inc., MA), and a mouse monoclonal anti-β-actin antibody (Sigma–Aldrich). Separated proteins were visualized using horseradish peroxidase with enhancement by chemiluminescence (GE Healthcare Bio-Sciences Corp., NJ).

Statistical Analysis

We used the computer program StatView 5.0 for Windows (SAS Institute, Cary, NC). Student's *t*-test was applied to compare results between two different groups. Repeated-measures ANOVA was used when comparing the in vivo tumor volume, and the in vitro cell migration in an individual group. One-way ANOVA was used when comparing the in vivo apoptosis, cell cycle progression, and liver metastases in an individual group. Statistical significance was assigned at $P < 0.05$.

RESULTS

Expression of SSTR2a and SSTR5 in NE-10 Allografts

Since effects of somatostatin analogs are mediated by expression of SSTR, we examined expression of the somatostatin receptor subtypes SSTR2 and SSTR5, to which SMS and SOM preferentially bind, respectively. Gene expression of SSTR2a and SSTR5 was observed in NE-10 allografts, but that of SSTR2b was not (Fig. 1).

Effects of ZOL, SMS and SOM as Single Agents and in Combination on Subcutaneously Inoculated NE-10 Allografts

Growth of NE-10 tumors in mice treated with ZOL, ZOL plus SMS, and ZOL plus SOM was significantly slowed compared to the saline control ($P = 0.003$, $P < 0.001$, and $P = 0.001$, respectively) (Fig. 2A). All treatments were well tolerated with maintenance of body weight (data not shown). We examined whether anti-tumor effects of each treatment were induced by apoptosis or cell cycle arrest by using TUNEL and Ki67 staining, respectively (Fig. $2B_1$). The AI was significantly increased in tumors of mice treated with ZOL, ZOL plus SMS, or ZOL plus SOM compared to the control (means: 9.2, 11.6, and 12.7, respectively, vs. 2.4) (Fig. $2B_2$). The KI was significantly decreased in tumors of mice treated with ZOL, ZOL plus SMS, or ZOL plus SOM compared to the control (means: 5.3, 8.3, and 4.2, respectively, vs. 15.9) (Fig. $2B_3$). The

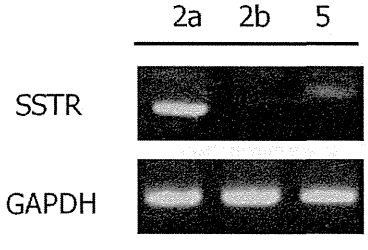

Fig. 1. Expression of SSTR2a, SSTR2b, and SSTR5 in NE-10 allograft by RT-PCR. Gene expression of SSTR2a, and SSTR5 was observed in the NE-10 allograft, but that of SSTR2b was not.

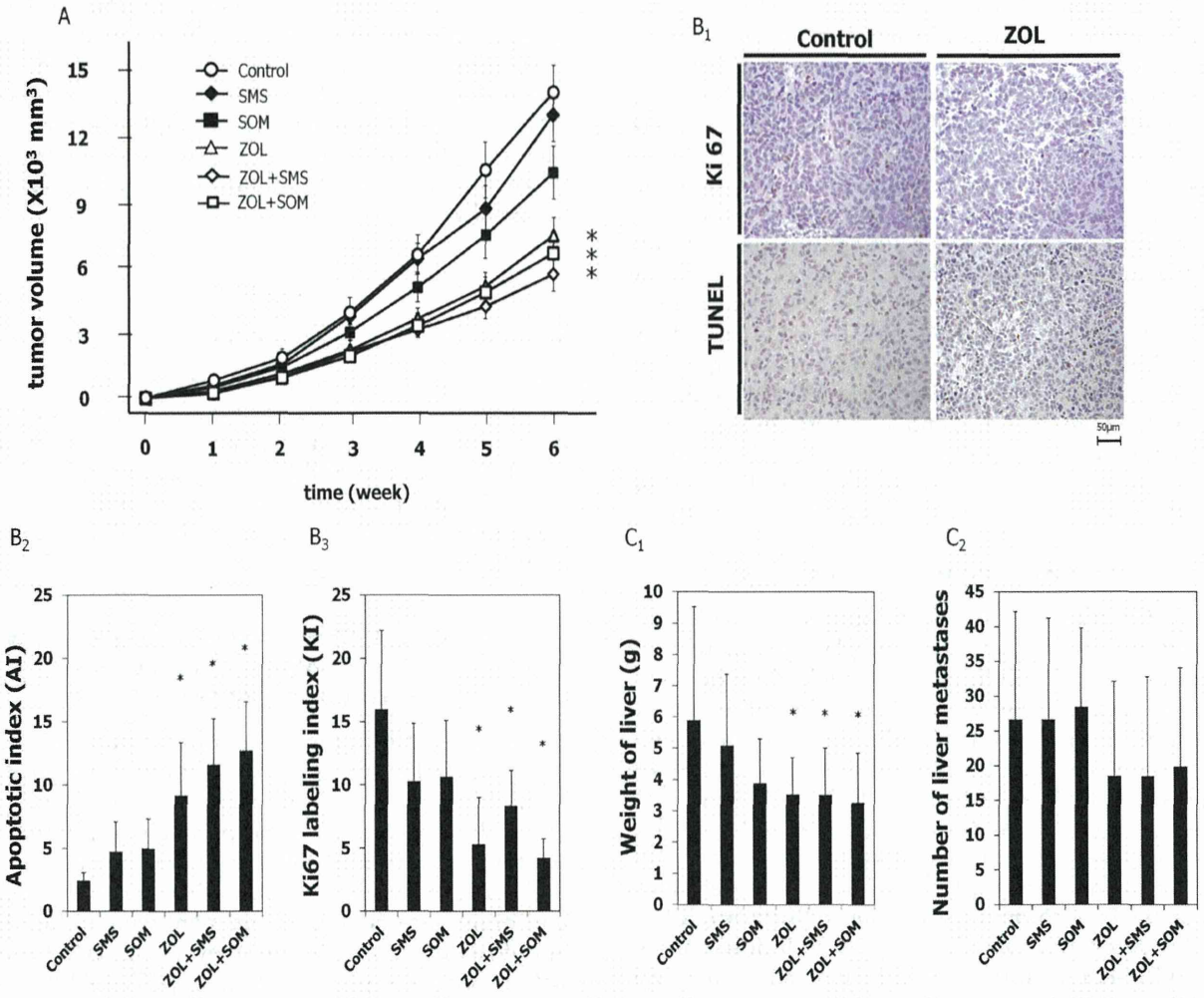

Fig. 2. Effects of ZOL, SMS, and SOM as single agents and in combination on subcutaneous inoculated NE-10 allografts. Six-week-old male BALB/c nude mice were castrated. After one week, 50 mg tissue fragments from the NE-10 allograft model were subcutaneously inoculated into the backs of mice. For 2 weeks, NE-10 tumors were allowed to grow to approximately more than 100 mm^3 before randomization into six treatment groups: control, ZOL, SMS, SOM, ZOL plus SMS, and ZOL plus SOM (n = 13/group). NE-10 allografts in each group were treated for 6 weeks. **A**: Growth of NE-10 tumors in mice treated with ZOL, ZOL plus SMS, and ZOL plus SOM was significantly slowed compared to the saline control ($P = 0.003$, $P < 0.001$, and $P = 0.001$, respectively). Data are means; bars ± SE; *, significantly different from control group ($P < 0.05$; repeated-measures ANOVA). **B**: Effects of ZOL, SMS and SOM as single agents and in combination on apoptosis and cell cycle progression. Immunohistochemical staining was done by using TUNEL and Ki67 staining (**B_1**). Apoptoic effects were measured by the number of TUNEL-positive cells per 1,000 cells, apoptoic index (AI). The AI was significantly increased in tumors from mice treated with ZOL, ZOL plus SMS, or ZOL plus SOM compared to the control (means: 9.2, 11.6, and 12.7, respectively, vs. 2.4) (**B_2**). Cell cycle progression was measured by the number of Ki67-positive cells per 1,000 cells (KI: Ki-67 labeling index). The KI was significantly decreased in tumors from mice treated with ZOL, ZOL plus SMS, or ZOL plus SOM compared to the control (means: 5.3, 8.3, and 4.2, respectively, vs. 15.9) (**B_3**). Data are means; bars ± SD; *, significantly different from control group ($P < 0.05$; one-way ANOVA). **C**: Effects of ZOL, SMS and SOM as single agents and in combination on liver metastases. The weights of livers having metastatic nodules in ZOL, ZOL plus SMS, or ZOL plus SOM were significantly lower than for the control (**C_1**). The numbers of metastatic nodules in these groups were not significantly different from the control (**C_2**). Data are means; bars ± SD. *, Significantly different from control group ($P < 0.05$; one-way ANOVA).

weights of livers having metastatic nodules in ZOL, ZOL plus SMS, or ZOL plus SOM were significantly lower than for the control (Fig. $2C_1$), but the numbers of metastatic nodules in these groups were not significantly different from the control (Fig. $2C_2$).

Effects of ZOL, SMS and SOM as Single Agents and in Combination on Growth of NE-CS Cells In Vitro

We investigated the inhibitory effects of ZOL, SMS, and SOM, alone and in combination on proliferation

of NE-CS cells. Cell viability was measured by the WST-8 assay when NE-CS cells were treated with various concentrations of ZOL, SMS and SOM (0.1–100 μmol/L) in the treatment groups for 24, 48 or 72 hr. For combinations, the same concentrations of ZOL and SMS or SOM were used. The IC50 for ZOL at 72 hr was 15.7 μmol/L, whereas those for ZOL plus SMS, and ZOL plus SOM were 14.1, and 13.5 μmol/L, respectively (Fig. 3A). The combination of ZOL and somatostatin analogs did not demonstrate synergistic effects (CI: 0.57–1.00). ZOL induced time- and dose-dependent proliferative inhibition of NE-CS cells (Fig. 3B). These effects of ZOL were reversed by 20 μmol/L of FOH (Fig. 3C).

ZOL Inhibits Cell Cycle Activity and Induces Apoptosis of NE-CS Cells

TUNEL-positive cells, indicated in red, increased with increased concentrations of ZOL. On the other hand, Ki-67-positive cells, colored green, decreased (Fig. 4A). We also analyzed the AI and KI with ZOL

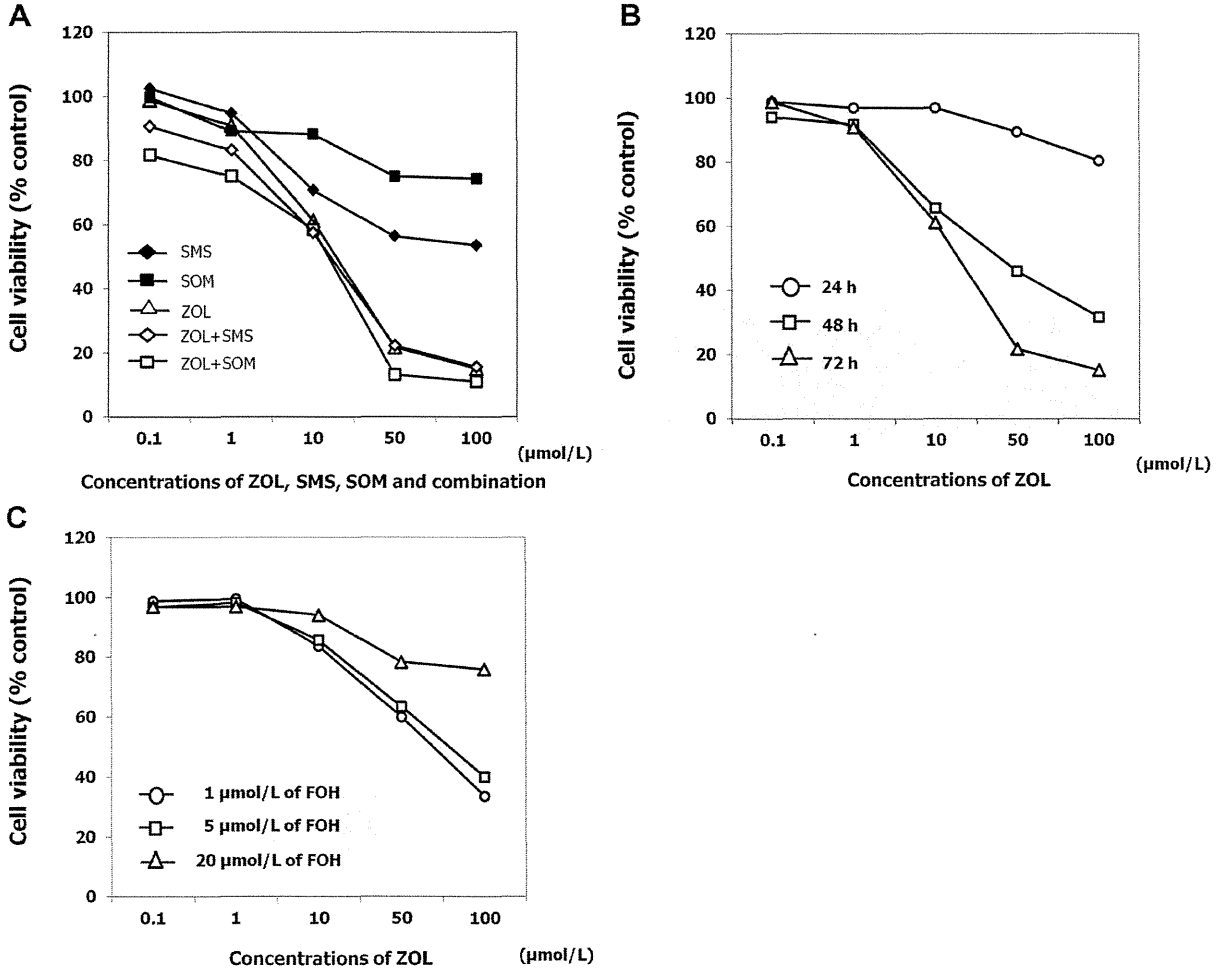

Fig. 3. Effects of ZOL, SMS and SOM as single agents and in combination on growth of NE-CS cells. Cell viability was measured by WST-8 assay when NE-CS cells were treated with various concentrations of ZOL, SMS and SOM (0.1–100 μmol/L) for 24, 48 or 72 hr. For combination, the same concentrations of ZOL and SMS or SOM were used. Cell viability was also measured when NE-CS cells were treated for 48 hr with the indicated concentrations (from 0.1 to 100 μmol/L) of ZOL plus 1, 5, and 20 μmol/L of farnesyl-pyrophosphate ammonium salt (FOH) (n = 5/group). **A**: Cell viability of NE-CS cells at 72 hr in each treatment group. The IC50 of ZOL at 72 hr for NE-CS cells was 15.7 μmol/L for ZOL, whereas it was 14.1 μmol/L for ZOL plus SMS, and 13.5 μmol/L for ZOL plus SOM. The combination of ZOL and somatostatin analogs did not create synergistic effects. **B**: Cell viability of NE-CS cells in time- and dose-dependent manners. ZOL induced time- and dose-dependent proliferative inhibition of NE-CS cells. **C**: Cell viability of NE-CS cells at 48 hr in ZOL plus FOH. ZOL-induced inhibition was reversed by 20 μmol/L of FOH.

concentrations of 0, 10, 50, and 100 μmol/L. The AI was significantly increased in ZOL 50, and 100 μmol/L compared to the control (means: 55.7 and 136.5, respectively, vs. 13.8) (Fig. 4B). The KI was significantly decreased in ZOL 10, 50, and 100 μmol/L compared to the control (means: 37.6, 22.8, and 1.3, respectively, vs. 68.7) (Fig. 4C).

ZOL Inhibits Migration of NE-CS Cells

In addition to effects of ZOL on cell cycle activity and apoptosis, we examined whether ZOL inhibited migration of NE-CS cells, using a Boyden chamber assay. NE-CS cells, with or without ZOL concentrations of 10, and 100 μmol/L, that migrated across the pores at 2, 4, 6 and 8 hr were counted. The numbers of cells migrating 1 mm^{-2} of membrane were significantly decreased in ZOL 10, and 100 μmol/L (Fig. 5A). When culture medium adding 20 μmol/L of FOH was incubated in upper chamber, the ZOL-induced inhibition was not appeared (Fig. 5B).

ZOL Utilizes the Ras/MAPK Pathway via the Mevalonate Pathway in NE-CS Cells

Since ZOL inhibits farnesyl-pyrophosphate synthetase in the mevalonate pathway and impairs prenylation of Ras, we evaluated the effects of ZOL on Ras activity. We used FOH, which potentially induces farnesylation of Ras. As evaluated by pull-down assay, 10, and 100 μmol/L inhibited Ras activation in NE-CS cells, and then the ZOL-induced inhibition was reversed by FOH (Fig. 6). We examined the effects of ZOL on Erk-1/2, which are the terminal proteins of the Ras/MAPK pathway. ZOL inhibited Erk1/2 phosphorylation as evaluated by Western blot assay.

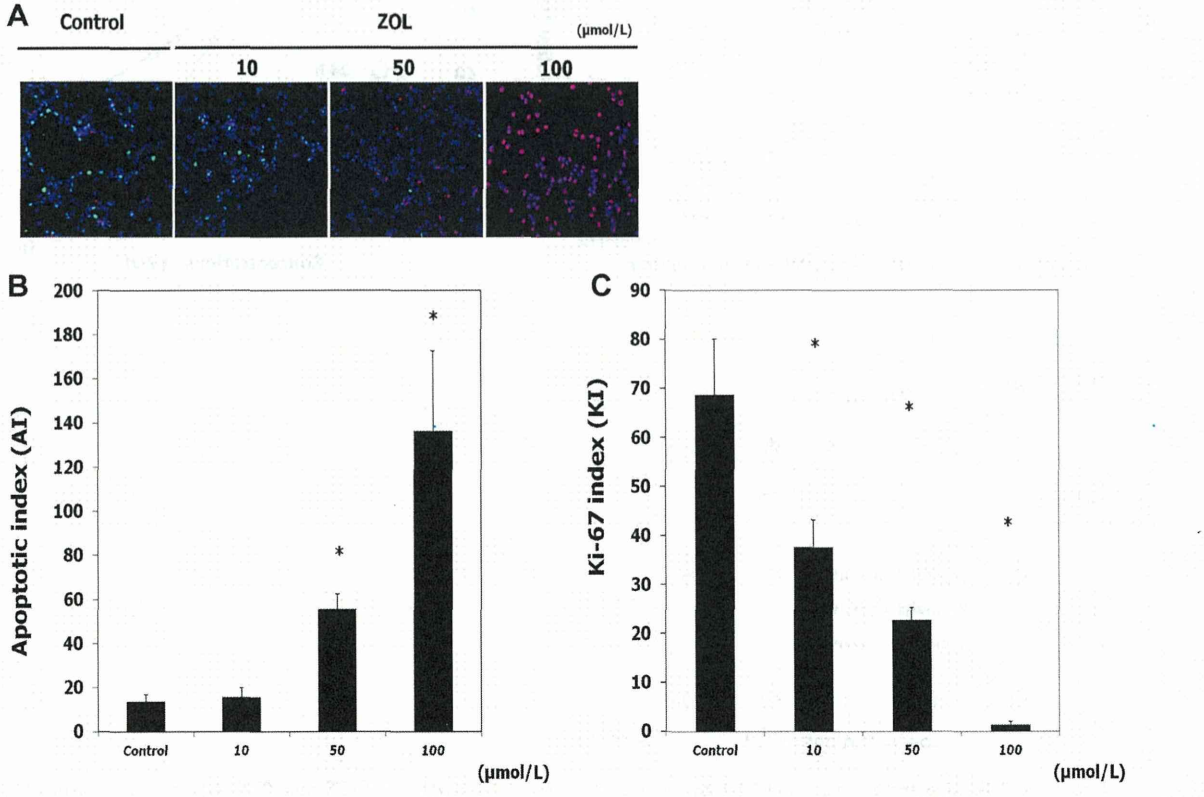

Fig. 4. Effects of ZOL on apoptosis and cell activity of NE-CS cells. **A**: TUNEL and anti-Ki67 immunofluorescence were used for NE-CS cells treated with ZOL concentrations of 0, 10, 50, and 100 μmol/L (n = 5/group). DAPI was used to visualize cell nuclei. TUNEL-positive cells, colored red, increased with increased concentrations of ZOL. On the other hand, Ki-67-positive cells, colored green, decreased. **B**: The numbers of TUNEL-positive cells per 1,000 cells apoptoic index (AI) were significantly increased in ZOL 50, and 100 μmol/L compared to the control (means: 55.7, and 136.5, respectively, vs. 13.8). Data are means; bars ± SD; *, significantly different from control group ($P < 0.001$; Student's *t*-test). **C**: The numbers of Ki67-positive cells per 1,000 cells (KI: Ki-67 labeling index) were significantly decreased in ZOL 10, 50, and 100 μmol/L compared to the control (means: 37.6, 22.8, and 1.3, respectively, vs. 68.7). Data are means; bars ± SD; *, significantly different from control group ($P < 0.001$; Student's *t*-test).

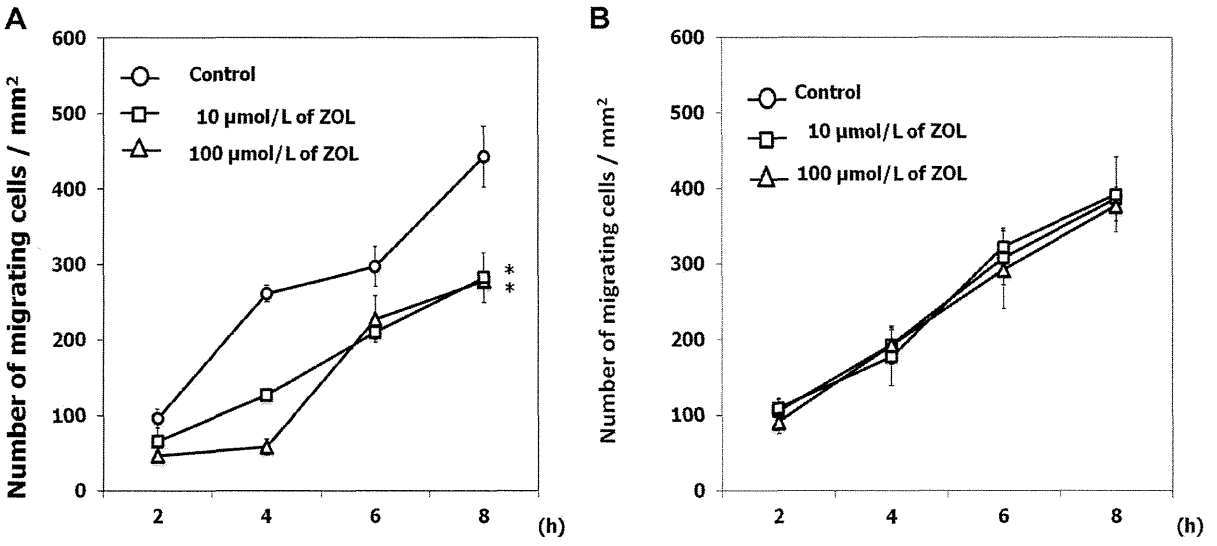

Fig. 5. Effects of ZOL on migration of NE-CS cells. Migration assay was performed by using a Boyden chamber (n = 3/group). **A**: In experiment I, NE-CS cells (1×10^5) were placed in the upper chamber with 100 μl of culture medium with or without ZOL (10, 100 μmol/L). In the lower chamber, 600 μl of culture medium was added. The numbers of cells migrating per 1 mm^{-2} of membrane were significantly decreased in ZOL 10, and 100 μmol/L. Data are means; bars ± SD; *, significantly different from the control ($P < 0.001$; repeated-measures ANOVA). B: In experiment 2, culture medium adding 20 μmol/L of farnesyl-pyrophosphate ammonium salt (FOH) was incubated in the upper chamber. The numbers of cells migrating 1 mm^{-2} of membrane were not significantly decreased in ZOL 10, and 100 μmol/L. Data are means; bars ± SD. *, Significantly different from the control ($P < 0.001$; repeated-measures ANOVA).

DISCUSSION

Inappropriate NE regulation in the prostate might facilitate carcinogenesis, proliferation and other tissue changes such as loss of basal cells, angiogenesis, and piling up of prostatic luminal epithelium and invasion, which are characteristic of prostatic carcinoma [20]. In addition, we previously demonstrated that secretions from NE cells stimulated prostatic cancer cells to achieve androgen-independent growth [21]. Androgen deprivation therapy induces an increased number of NE cells in prostate cancer and the frequency and density of NE cells are more pronounced in CRPC [22]. Thus, the control of NE cells might be important for establishing a treatment strategy for CRPC.

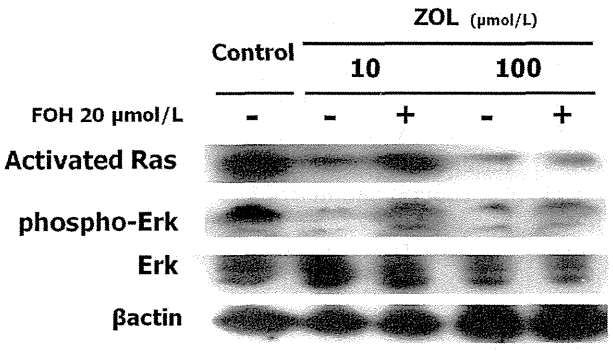

Fig. 6. Effects of ZOL on Ras/MAPK pathway of NE-CS cells. We used farnesyl-pyrophosphate ammonium salt (FOH), which potentially induces farnesylation of Ras. Ras activity was evaluated by pull-down assay, and Erk activity by Western blot assay. As evaluated by pull-down assay, 10, and 100 μmol/L ZOL inhibited Ras activation in NE-CS cells, and then the ZOL-induced inhibition was reversed by FOH. ZOL inhibited Erk1/2 phosphorylation in NE-CS cells as evaluated by Western blot assay.

Somatostatin analogs have been used clinically used to treat NE tumors [23]. SMS and lanreotide, which have high affinity to SSTR2a, have been demonstrated to reduce excessive hormone production and accompanying symptoms from carcinoid tumors and pancreatic endocrine tumors such as glucagonoma, VIPoma and gastrinoma [14]. The anticancer effect may be the result of antiproliferative and apoptoic actions through direct and indirect mechanisms. The direct mechanism is mediated by SSTR on tumor cells, and suppression of secretion of several growth factors such as insulin-like growth factor-1 (IGF-1) may also indirectly inhibit the tumor growth [24–26]. In this study, in spite of the expression of SSTR2a and SSTR5 in our NE carcinoma models, we failed to find significant antiproliferative effects of SMS or SOM monotherapy in vitro or in vivo. In addition, the combination therapy with ZOL did not create a synergistic effect. Although, the exact reason is unclear, both

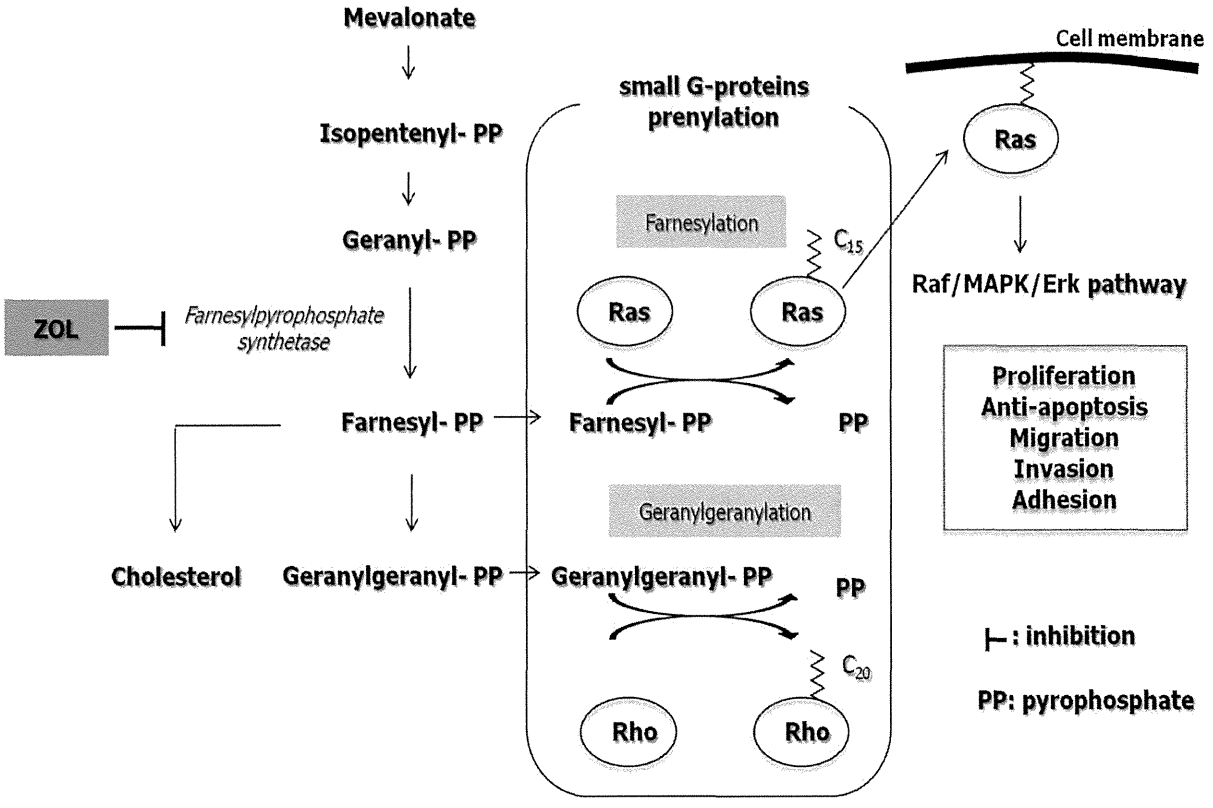

Fig. 7. Schematic representation of the mevalonate pathway and proposed mechanism of anti-tumor effects of zoledronic acid in prostatic NE carcinoma.

SMS and SOM might be insufficient to control our NE carcinoma models through autocrine, paracrine and endocrine regulation via SSTRs.

Our results suggest that ZOL induces time- and dose-dependent antiproliferative and apoptoic effects in prostatic NE carcinoma. The observed anticancer activity was exerted at ZOL IC50 levels of from 15.8 to 36.0 μmol/L. In addition, the drug reduced migration by 8 hr in vitro even at the 10 μmol/L concentration, and the time and dose did not seem to affect the viability of cells. These effects were caused by disruption of prenylation of Ras proteins as a result of farnesyl-pyrophosphate synthetase inhibition, disrupting the downstream MAPK/Erk signaling pathway (Fig. 7). Farnesyl-pyrophosphate synthetase is a key enzyme in the mevalonate pathway, which produces essential lipid molecules such as cholesterol, farnesyl-pyrophosphate and geranylgeranyl-pyrophosphate [27]. Small G proteins need prenylation to link to the inner surface of the cell membrane and function in signal translation [28]. Prenylation of small G proteins involves farnesylation, which provides a 15-carbon isoprenoid moiety with Ras, and geranylgeranylation, which provides a 20-carbon isoprenoid moiety with Rap Rac or Rho [27,28]. Ras is the most thoroughly characterized member of the small G proteins involved in key oncogenic cellular processes such as proliferation, anti-apoptosis, migration, invasion and adhesion (Fig. 7). Therefore, it is anticipated that ZOL disturbing prenylation of Ras will induce multifactorial anticancer effects in cancer cells.

Several studies had shown that ZOL induces apoptosis via impaired prenylation of small G proteins in various cancer cells, including prostate [12,29–31], breast [32,33], myeloma [34], colon [35], and lung cancer cell lines [36]. Caraglia et al. [12] reported the effects of the combination of ZOL and farnesyl-transferase inhibitor R115777 on PC3 and DU145 prostate cancer cell lines. These effects paralleled disruption of Ras/MAPK/Erk and Akt survival pathways, which consequently decreased phosphorylation of both mitochondrial bcl-2 and bad proteins, and caspase activation. These findings may support our results indicating that ZOL induced apoptosis of NE cells. Recents studies have shown that impaired geranylgeranylation on other small G proteins such as Rap1 [29,34] and RhoA [32] is also crucial for the association with these apoptotic actions induced by ZOL.

We also demonstrated that ZOL induced cell cycle arrest of the NE carcinoma cells. Both in vitro, and in

vivo, ZOL reduced the numbers of Ki67-positive cells during all active phases of the cell cycle (G1, S, G2, and M). ZOL has been shown to reduce the expression of cyclin D1 and cyclin E in osteosarcoma cells, resulting in a cell cycle block at G1, and S [37]. In addition, experiments using leukemia cells have shown that ZOL can also reduce the expression of cyclin D3 and cyclin B, resulting in a cell cycle block at G2-M [38]. These actions are suggested to occur in a p53-independent manner followed by subsequent apoptosis. Our results indicated that ZOL inhibited the cell cycle of NE cells.

Moreover, we demonstrated that ZOL inhibited migration of NE-CS cells. It decreased the weights of livers having metastatic nodules in castrated NE-10 allografts, which means to suppress liver metastases. Likewise, Hiraga et al. [39] reported that 1 μmol/L ZOL significantly inhibited cell invasion in a breast cancer cell line (4T1/Luc), which consequently led to suppression of liver and bone metastases. Similar results were also observed in prostate cancer cell lines LNCaP, PC3, and DU145 31. In addition, Coxon et al. [40] reported an inhibitory effect of 1 μmol/L ZOL on adhesion to mineralized matrix in PC3, and DU145 cells. Although the exact mechanisms underlying these effects remain unclear, it is suggested that ZOL could inhibit several matrix metalloproteinase or adhesion molecules via impairment of prenylation of small G proteins. It is noteworthy that ZOL also inhibits essential steps for the spread of cancer cells. In addition, recent reports have shown that ZOL indirectly exerts anticancer effects via elevated function of gamma delta T cells [41,42]. It is suggested that accumulation of isopentenyl-pyrophosphate caused by ZOL may be involved in activation of gamma delta T cells [43].

There are some limitations in this study. The NE-10 allograft and the NE-CS cell line were derived from the mouse prostate. The role of human NE cells in human prostate cancer may be different from that of mouse NE cells. In addition, the characteristics of the established cell line, NE-CS, could be different from those of the original NE-10 allograft because cells suitable for survival in vitro were selected during establishment of the cell line. However, there are no ideal human lines for which both in vitro, and in vivo NE carcinoma models are available. In addition, the concentration of ZOL that induced anticancer effects in our experiments was high in comparison to the peak plasma levels (393 ± 100 ng/ml) usually achieved by intravenous infusion in patients [44]. Anticancer effects of ZOL might be considered to be exerted basically in bone metastatic lesions in which high concentrations of ZOL are achieved.

In patients with bone metastasis of prostate cancer, ZOL is commonly used for relieving pain and preventing skeletal-related events. This study revealed effects of ZOL on NE cells, potential triggers of prostate cancer leading to CRPC. Regulating the microenvironment between NE cells and prostate cancer cells may result in benefits to patients who do not have clinically detected bone metastasis. We believe that our results support the clinical rationale for earlier proactive use of ZOL, though further studies will be needed to confirm this.

CONCLUSION

We examined the in vitro, and in vivo anti-tumor effects of ZOL and somatostatin analogs (SMS and SOM) on NE carcinoma models. Our results indicate that ZOL, but not SMS or SOM, induces apoptosis and inhibition of proliferation and migration through impaired prenylation of Ras. Our findings support the possibility that ZOL could be used in the early phase for controlling NE cells which may trigger progression of prostate cancer to CRPC.

REFERENCES

1. Jemal A, Bray F, Center MM, Ferlay J, Ward E, Forman D. Global cancer statistics. CA Cancer J Clin 2011;61(2):69–90.
2. Heidenreich A, Aus G, Bolla M, Joniau S, Matveev VB, Schmid HP, Zattoni F. EAU guidelines on prostate cancer. Eur Urol 2008;53(1):68–80.
3. Debes JD, Tindall DJ. Mechanisms of androgen-refractory prostate cancer. N Engl J Med 2004;351(15):1488–1490.
4. di Sant'Agnese PA. Neuroendocrine differentiation in prostatic carcinoma: An update. Prostate Suppl 1998;8:74–79.
5. Ito T, Yamamoto S, Ohno Y, Namiki K, Aizawa T, Akiyama A, Tachibana M. Up-regulation of neuroendocrine differentiation in prostate cancer after androgen deprivation therapy, degree and androgen independence. Oncol Rep 2001;8(6): 1221–1224.
6. Hirano D, Okada Y, Minei S, Takimoto Y, Nemoto N. Neuroendocrine differentiation in hormone refractory prostate cancer following androgen deprivation therapy. Eur Urol 2004;45(5): 586–592; discussion 592.
7. Masumori N, Thomas TZ, Chaurand P, Case T, Paul M, Kasper S, Tsukamoto T, Shappell SB, Matusik RJ. A probasin–Large T antigen transgenic mouse line develops prostate adenocarcinoma and neuroendocrine carcinoma with metastatic potential. Cancer Res 2001;61(5):2239–2249.
8. Masumori N, Tsuchiya K, Tu WH, Lee C, Kasper S, Tsukamoto T, Shappell SB, Matusik RJ. An allograft model of androgen independent prostatic neuroendocrine carcinoma derived from a large probasin promoter-T antigen transgenic mouse line. J Urol 2004;171(1):439–442.
9. Uchida K, Masumori N, Takahashi A, Itoh N, Tsukamoto T. Characterization of prostatic neuroendocrine cell line established from neuroendocrine carcinoma of transgenic mouse allograft model. Prostate 2005;62(1):40–48.

10. Uchida K, Masumori N, Takahashi A, Itoh N, Kato K, Matusik RJ, Tsukamoto T. Murine androgen-independent neuroendocrine carcinoma promotes metastasis of human prostate cancer cell line LNCaP. Prostate 2006;66(5):536–545.
11. Saad F, Gleason DM, Murray R, Tchekmedyian S, Venner P, Lacombe L, Chin JL, Vinholes JJ, Goas JA, Chen B. A randomized, placebo-controlled trial of zoledronic acid in patients with hormone-refractory metastatic prostate carcinoma. J Natl Cancer Inst 2002;94(19):1458–1468.
12. Caraglia M, Marra M, Leonetti C, Meo G, D'Alessandro AM, Baldi A, Santini D, Tonini G, Bertieri R, Zupi G, Budillon A, Abbruzzese A. R115777 (Zarnestra)/Zoledronic acid (Zometa) cooperation on inhibition of prostate cancer proliferation is paralleled by Erk/Akt inactivation and reduced Bcl-2 and bad phosphorylation. J Cell Physiol 2007;211(2):533–543.
13. Patel YC. Somatostatin its receptor, family Front Neuroendocrinol 1999;20(3):157–198.
14. Hejna M, Schmidinger M, Raderer M. The clinical role of somatostatin analogs as antineoplastic agents: Much ado about nothing? Ann Oncol 2002;13(5):653–668.
15. Reubi JC, Waser B, Schaer JC, Laissue JA. Somatostatin receptor SSTR1–SSTR5 expression in normal and neoplastic human tissues using receptor autoradiography with subtype-selective ligands. Eur J Nucl Med 2001;28(7):836–846.
16. Halmos G, Schally AV, Sun B, Davis R, Bostwick DG, Plonowski A. High expression of somatostatin receptors and messenger ribonucleic acid for its receptor subtypes in organ-confined and locally advanced human prostate cancers. J Clin Endocrinol Metab 2000;85(7):2564–2571.
17. Bruns C, Lewis I, Briner U, Meno-Tetang G, Weckbecker G. SO M230 a novel somatostatin peptidomimetic with broad somatotropin release inhibiting factor (SRIF) receptor binding and a unique antisecretory profile. Eur J Endocrinol 2002 ;146(5):707–716.
18. Chou TC, Talalay P. Quantitative analysis of dose-effect relationships: The combined effects of multiple drugs or enzyme inhibitors. Adv Enzyme Regul 1984;22:27–55.
19. Topaly J, Zeller WJ, Fruehauf S. Synergistic activity of the new ABL-specific tyrosine kinase inhibitor STI571 and chemotherapeutic drugs on BCR-ABL-positive chronic myelogenous leukemia cells. Leukemia 2001;15(3):342–347.
20. Bok RA, Small EJ. Bloodborne biomolecular markers in prostate cancer development and progression. Nat Rev Cancer 2002;2(12):918–926.
21. Jin RJ, Wang Y, Masumori N, Ishii K, Tsukamoto T, Shappell SB, Hayward SW, Kasper S, Matusik RJ. NE-10 neuroendocrine cancer promotes the LNCaP xenograft growth in castrated mice. Cancer Res 2004;64(15):5489–5495.
22. Weinstein MH, Partin AW, Veltri RW, Epstein JI. Neuroendocrine differentiation in prostate cancer: Enhanced prediction of progression after radical prostatectomy. Hum Pathol 1996; 27(7):683–687.
23. Sciarra A, Bosman C, Monti G, Gentile V, Autran Gomez AM, Ciccariello M, Pastore A, Salvatori G, Fattore F, Di Silverio F. Somatostatin analogs and estrogens in the treatment of androgen ablation refractory prostate adenocarcinoma. J Urol 2004;172(5 Pt 1):1775–1783.
24. Pawlikowski M, Melen-Mucha G. Perspectives of new potential therapeutic applications of somatostatin analogs. Neuro Endocrinol Lett 2003;24(1–2):21–27.
25. van der Hoek J, van der Lelij AJ, Feelders RA, de Herder WW, Uitterlinden P, Poon KW, Boerlin V, Lewis I, Krahnke T, Hofland LJ, Lamberts SW. The somatostatin analogue SOM230, compared with octreotide, induces differential effects in several metabolic pathways in acromegalic patients. Clin Endocrinol (Oxf) 2005;63(2):176–184.
26. Schmid HA. Pasireotide (SOM230): Development, mechanism of action and potential applications. Mol Cell Endocrinol 2008;286(1–2):69–74.
27. Kavanagh KL, Guo K, Dunford JE, Wu X, Knapp S, Ebetino FH, Rogers MJ, Russell RG, Oppermann U. The molecular mechanism of nitrogen-containing bisphosphonates as antiosteoporosis drugs. Proc Natl Acad Sci USA 2006;103(20):7829–7834.
28. Hougland JL, Fierke CA. Getting a handle on protein prenylation. Nat Chem Biol 2009;5(4):197–198.
29. Nogawa M, Yuasa T, Kimura S, Kuroda J, Segawa H, Sato K, Yokota A, Koizumi M, Maekawa T. Zoledronic acid mediates Ras-independent growth inhibition of prostate cancer cells. Oncol Res 2005;15(1):1–9.
30. Fabbri F, Brigliadori G, Carloni S, Ulivi P, Vannini I, Tesei A, Silvestrini R, Amadori D, Zoli W. Zoledronic acid increases docetaxel cytotoxicity through pMEK and Mcl-1 inhibition in a hormone-sensitive prostate carcinoma cell line. J Transl Med 2008;6:43.
31. Mani J, Vallo S, Barth K, Makarevic J, Juengel E, Bartsch G, Wiesner C, Haferkamp A, Blaheta RA. Zoledronic acid influences growth, migration and invasive activity of prostate cancer cells in vitro. Prostate Cancer Prostatic Dis 2012;15(3):250–255.
32. Denoyelle C, Hong L, Vannier JP, Soria J, Soria C. New insights into the actions of bisphosphonate zoledronic acid in breast cancer cells by dual RhoA-dependent and -independent effects. Br J Cancer 2003;88(10):1631–1640.
33. Ottewell PD, Lefley DV, Cross SS, Evans CA, Coleman RE, Holen I. Sustained inhibition of tumor growth and prolonged survival following sequential administration of doxorubicin and zoledronic acid in a breast cancer model. Int J Cancer 2009;126(2):522–532.
34. Guenther A, Gordon S, Tiemann M, Burger R, Bakker F, Green JR, Baum W, Roelofs AJ, Rogers MJ, Gramatzki M. The bisphosphonate zoledronic acid has antimyeloma activity in vivo by inhibition of protein prenylation. Int J Cancer 2010;126(1):239–246.
35. Sewing L, Steinberg F, Schmidt H, Goke R. The bisphosphonate zoledronic acid inhibits the growth of HCT-116 colon carcinoma cells and induces tumor cell apoptosis. Apoptosis 2008; 13(6):782–789.
36. Tannehill-Gregg SH, Levine AL, Nadella MV, Iguchi H, Rosol TJ. The effect of zoledronic acid and osteoprotegerin on growth of human lung cancer in the tibias of nude mice. Clin Exp Metast 2006;23(1):19–31.
37. Kubista B, Trieb K, Sevelda F, Toma C, Arrich F, Heffeter P, Elbling L, Sutterluty H, Scotlandi K, Kotz R, Micksche M, Berger W. Anticancer effects of zoledronic acid against human osteosarcoma cells. J Orthop Res 2006;24(6):1145–1152.
38. Kuroda J, Kimura S, Segawa H, Kobayashi Y, Yoshikawa T, Urasaki Y, Ueda T, Enjo F, Tokuda H, Ottmann OG, Maekawa T. The third-generation bisphosphonate zoledronate synergistically augments the anti-pH + leukemia activity of imatinib mesylate. Blood 2003;102(6):2229–2235.
39. Hiraga T, Williams PJ, Ueda A, Tamura D, Yoneda T. Zoledronic acid inhibits visceral metastases in the 4T1/Luc mouse breast cancer model. Clin Cancer Res 2004;10(13):4559–4567.

40. Coxon JP, Oades GM, Kirby RS, Colston KW. Zoledronic acid induces apoptosis and inhibits adhesion to mineralized matrix in prostate cancer cells via inhibition of protein prenylation. BJU Int 2004;94(1):164–170.
41. Marten A, Lilienfeld-Toal M, Buchler MW, Schmidt J. Zoledronic acid has direct antiproliferative and antimetastatic effect on pancreatic carcinoma cells and acts as an antigen for delta2 gamma/delta T cells. J Immunother 2007;30(4):370–377.
42. Sato K, Kimura S, Segawa H, Yokota A, Matsumoto S, Kuroda J, Nogawa M, Yuasa T, Kiyono Y, Wada H, Maekawa T. Cytotoxic effects of gammadelta T cells expanded ex vivo by a third generation bisphosphonate for cancer immunotherapy. Int J Cancer 2005;116(1):94–99.
43. Roelofs AJ, Jauhiainen M, Monkkonen H, Rogers MJ, Monkkonen J, Thompson K. Peripheral blood monocytes are responsible for gamma delta T cell activation induced by zoledronic acid through accumulation of IPP/DMAPP. Br J Haematol 2009;144(2):245–250.
44. Reid IR, Brown JP, Burckhardt P, Horowitz Z, Richardson P, Trechsel U, Widmer A, Devogelaer JP, Kaufman JM, Jaeger P, Body JJ, Brandi ML, Broell J, Di Micco R, Genazzani AR, Felsenberg D, Happ J, Hooper MJ, Ittner J, Leb G, Mallmin H, Murray T, Ortolani S, Rubinacci A, Saaf M, Samsioe G, Verbruggen L, Meunier PJ. Intravenous zoledronic acid in postmenopausal women with low bone mineral density. N Engl J Med 2002;346(9):653–661.

HEPATOLOGY
Official Journal of the American Association for the Study of Liver Diseases

Differentiation Capacity of Hepatic Stem/Progenitor Cells Isolated From D-Galactosamine-Treated Rat Livers

Norihisa Ichinohe,[1] Naoki Tanimizu,[1] Hidekazu Ooe,[1] Yukio Nakamura,[1,2] Toru Mizuguchi,[2] Junko Kon,[1] Koichi Hirata,[2] and Toshihiro Mitaka[1]

Oval cells and small hepatocytes (SHs) are known to be hepatic stem and progenitor cells. Although oval cells are believed to differentiate into mature hepatocytes (MHs) through SHs, the details of their differentiation process are not well understood. Furthermore, it is not certain whether the induced cells possess fully mature functions as MHs. In the present experiment, we used Thy1 and CD44 to isolate oval and progenitor cells, respectively, from D-galactosamine-treated rat livers. Epidermal growth factor, basic fibroblast growth factor, or hepatocyte growth factor could trigger the hepatocytic differentiation of sorted $Thy1^+$ cells to form epithelial cell colonies, and the combination of the factors stimulated the emergence and expansion of the colonies. Cells in the $Thy1^+$-derived colonies grew more slowly than those in the $CD44^+$-derived ones *in vitro* and *in vivo* and the degree of their hepatocytic differentiation increased with CD44 expression. Although the induced hepatocytes derived from $Thy1^+$ and $CD44^+$ cells showed similar morphology to MHs and formed organoids from the colonies similar to those from SHs, many hepatic differentiated functions of the induced hepatocytes were less well performed than those of mature SHs derived from the healthy liver. The gene expression of cytochrome P450 1A2, tryptophan 2,3-dioxygenase, and carbamoylphosphate synthetase I was lower in the induced hepatocytes than in mature SHs. In addition, the protein expression of CCAAT/enhancer-binding protein alpha and bile canalicular formation could not reach the levels of production of mature SHs. *Conclusion*: The results suggest that, although $Thy1^+$ and $CD44^+$ cells are able to differentiate into hepatocytes, the degree of maturation of the induced hepatocytes may not be equal to that of healthy resident hepatocytes. (HEPATOLOGY 2012; 57:1192-1202)

The liver normally exhibits a very low level of cell turnover, but when loss of mature hepatocytes (MHs) occurs, a rapid regenerative response is elicited from all cell types in the liver to restore the organ to its initial state. The loss may occur as a result of toxic injury, viral infection, trauma, or surgical resection. Because hepatocytes are the major functional cells of the liver, large-scale hepatocytic loss becomes a trigger for regeneration, and replication of existing hepatocytes is generally the quickest, most efficient way to compensate for the lost functions. However, when the replication of hepatocytes is delayed or entirely inhibited, hepatic stem/progenitor cells (HPCs) are activated.[1-3] As HPCs, oval cells and small hepatocytes (SHs) are well known. Oval cells were first reported to be cells that possessed an ovoid nucleus and

Abbreviations: Abs, antibodies; AFP, alpha-fetoprotein; Alb, albumin; BC, bile canaliculus; bFGF, basic fibroblast growth factor; BrdU, 5-bromo-2'-deoxyuridine; BW, body weight; CPS-I, carbamoylphosphate synthetase I; CK, cytokeratin; C/EBP, CCAAT/enhancer-binding protein; CYP1A2, cytochrome P450 1A2; 3D, three-dimensional; DPPIV, dipeptidylpeptidase IV; ECM, extracellular matrix; EGF, epidermal growth factor; FD, fluorescent diacetate; FGF, fibroblast growth factor; GalN, D-galactosamine; HA, hyaluronic acid; HGF, hepatocyte growth factor; HNF, hepatocyte nuclear factor; HPCs, hepatic stem/progenitor cells; ICC, immunocytochemistry; INF-γ, interferon-gamma; IP, intraperitoneally; LI, labeling index; MH, mature hepatocyte; mRNA, messenger RNA; PBS, phosphate-buffered saline; PH, partial hepatectomy; qPCR, quantitative polymerase chain reaction; RET, retrorsine; SH, small hepatocyte; TAT, tyrosine aminotransferase; TGF, transforming growth factor; TNF-α, tumor necrosis factor alpha; TDO, tryptophan 2,3-dioxygenase;

From the [1]Department of Tissue Development and Regeneration, the Research Institute for Frontier Medicine, and [2]First Department of Surgery, Sapporo Medical University School of Medicine, Sapporo, Japan.

Received January 31, 2012; accepted September 8, 2012.

This work was supported by the Ministry of Education, Culture, Sports, Science, and Technology, Japan, Grant-in-Aid for Scientific Research (C) (19566021; to N.I.), Grants-in-Aid for Young Scientists (B) (22790385, to N.I.; and 19790294, to J.K.), a grant from the Yuasa Memorial Foundation (to T.M.), and Grants-in-Aid for Scientific Research (B) (22390259, to K.H.; and 21390365, to T.M.), a program for developing the supporting system for upgrading the education and research (to T.M.).

Dr. Kon is currently affiliated with Gene Techno Science Co. Ltd., Sapporo, Japan.

scant cytoplasm.[4] The appearance of oval cells has been reported in rat livers treated with hepatotoxins, such as 2-acetylaminofluorene (2-AAF), combined with partial hepatectomy (PH) and D-galactosamine (GalN).[1,5–7] In GalN-induced rat liver injury, it has been shown that oval cells appear in the periportal area and differentiate into MHs through basophilic small-sized ones.[8,9] Oval cells show a wide range of phenotypic heterogeneity, and cytokeratins (CKs) 7 and 19, alpha-fetoprotein (AFP), CD34, c-kit, and Thy1 have been reported as markers for them.[1,2,5–7]

On the other hand, SHs are a subpopulation of hepatocytes, and cells isolated from healthy adult rats[10,11] and human livers[12] can clonally proliferate to form colonies and differentiate into MHs *in vitro*.[11,13] Recently, we identified CD44 as a specific marker of SHs.[14] In GalN-treated rat livers, $CD44^+$ cells appear near the periportal area between $Thy1^+$ oval cells and resident hepatocytes soon after the emergence of $Thy1^+$ oval cells.[15] In addition, we previously showed that $Thy1^+$ oval cells differentiate into hepatocytes through $CD44^+$ cells.[15,16] Our data suggested that cells sequentially converted from $Thy1^+CD44^-$ to $Thy1^+CD44^+$ and then to $Thy1^-CD44^+$ cells during the process of hepatocytic differentiation of oval cells.[15,16] Furthermore, sorted $Thy1^+$ and $CD44^+$ cells could repopulate host livers when they were transplanted into rat livers treated with retrorsine (RET) and two-thirds PH.

Although most oval cells are thought to differentiate into MHs, the details of their differentiation process, such as factors for hepatic commitment, characteristics of intermediate cells, and their fates are not well understood. In addition, it has not been elucidated whether the induced hepatocytes differentiate to possess the same capabilities as MHs. In the present experiment, we aimed to clarify which factors might induce hepatocytic differentiation of $Thy1^+$ cells and to examine how $Thy1^+$ cells could differentiate into hepatocytes through $CD44^+$ cells. In addition, we examined whether the $Thy1^+$ and $CD44^+$ cells could differentiate into fully MHs, as with those in the healthy adult liver.

Materials and Methods

Animals and Liver Injury Model. Male F344 rats (dipeptidylpeptidase IV $[DPPIV]^+$ strain; Sankyo Lab Service Corporation, Inc., Tokyo, Japan), weighing 150-200 g, were used. All animals received humane care, and the experimental protocol was approved by the committee on laboratory animals according to Sapporo Medical University guidelines. For GalN-injured livers, GalN (75 mg/100 g body weight [BW] dissolved in phosphate-buffered saline [PBS]; Acros, Geel, Belgium) was intraperitoneally (IP) administered.[14] For the transplantation experiment, female F344 rats ($DPPIV^-$ strain; Charles River Laboratories, Wilmington, MA) were (IP) given two injections of RET (30 mg/kg BW; Sigma-Aldrich Chemical Co., St. Louis, MO), 2 weeks apart,[17] and 4 weeks after the second injection, two-thirds PH was performed (RET/PH liver). Sorted $DPPIV^+$ cells (5×10^5 cells/0.5 mL) were transplanted into RET/PH livers ($DPPIV^-$) through the spleen (at least 3 rats per group).

Isolation and Culture of Cells. Rats were used to isolate hepatic cells by the collagenase perfusion method, as previously described.[18] After perfusion, the cell suspension was centrifuged at $50 \times g$ for 1 minute. The supernatant and the precipitate were used for sorting $Thy1^+$ and $CD44^+$ cells and preparing MHs, respectively. The procedure used for cell sorting was as previously described,[15] with some modifications. Antibodies (Abs) used for cell sorting are listed in Supporting Table 1. $Thy1^+CD44^+$ cells were sorted from $CD44^+$ cell and $Thy1^+$ cell fractions by using anti-Thy1 or CD44 Abs, respectively, and both were pooled. Furthermore, $Thy1^+$ and $CD44^+$ cells were also separated from $CD44^-$ and $Thy1^-$ cell fractions, respectively. After the number of viable cells was counted, 1×10^5 viable cells were plated in 12-well plates (Corning Inc., Corning, NY) and cultured in the medium listed in Supporting Table 2. The medium was replaced with fresh medium thrice-weekly.

To examine whether cells in the colonies could fully differentiate into MHs and form functional bile canaliculi (BCs), $Thy1^+CD44^-$ and $Thy1^-CD44^+$ cells sorted from GalN-D3 and SHs derived from a healthy liver were cultured for 10 days. Thereafter, some dishes were treated with Matrigel (BD Biosciences, San Diego, CA) for 10 days. To enhance the organoid formation of the colonies, as previously reported,[19]

Address reprint requests to: Norihisa Ichinohe, D.D.S., Ph.D., Department of Tissue Development and Regeneration, Research Institute for Frontier Medicine, Sapporo Medical University School of Medicine, South-1, West-17, Chuo-ku, Sapporo 060-8556, Japan. E-mail: nichi@sapmed.ac.jp; fax: +81-11-615-3099.

View this article online at wileyonlinelibrary.com.
DOI 10.1002/hep.26084
Potential conflict of interest: Nothing to report.
Additional Supporting Information may be found in the online version of this article.

colonies were separated from dishes by using Cell Dissociation Solution (Sigma-Aldrich), and colonies (2×10^3) were replated on collagen-coated dishes. Cells were cultured in the induction medium (Supporting Table 2) for 14 days. Cloning rings were used to isolate total RNA of each colony. At least two separate experiments were performed, and more than five colonies were investigated.

GeneChip Analysis, RNA Isolation, and Real-Time Polymerase Chain Reaction. Details are shown in the Supplementary Methods.

Immunostaining. For detecting $CD44^+$ colonies, cells were fixed with cold absolute ethanol at 10 days after plating, and immunocytochemistry (ICC) for CD44 was carried out. Details of staining were previously reported.[15] The numbers of $CD44^+$ colonies at days 5 and 10 were counted, and positivity was calculated. Three separate experiments were performed. To measure the labeling index (LI), 40 μM of 5-bromo-2'-deoxyuridine (BrdU) were added to the medium 24 hours before fixation. In double ICC for CD44 and BrdU, a combination of the avidin-biotin peroxidase complex method (Vectastain ABC Elite Kit; Vector Laboratories Inc., Burlingame, CA) and the alkaline phosphatase method was used. For fluorescent immunohistochemistry, sliced liver samples were frozen using isopentane/liquid nitrogen, and materials were kept at −80°C until use. All Abs used for immunostaining are listed in Supporting Table 1. Sections were embedded with 90% glycerol including 0.01% *p*-phenylenediamine and 4,6-diamidino-2-phenylindole. A confocal laser microscope (Olympus, Tokyo, Japan) was used for observation, and findings were analyzed using DP Manager (Olympus).

Treatment With Fluorescein Diacetate. As previously reported,[20] fluorescein diacetate (FD; Sigma-Aldrich) was dissolved in dimethyl sulfoxide, and the solution was diluted with the culture medium. Then, 0.25% FD was added to the medium, and the dish was rinsed three times with warm PBS. Fluorescent images were immediately photographed using a phase-contrast microscope equipped with a fluorescence device (Olympus).

Enzyme Histochemisty for DPPIV. To identify donor cells, enzyme histochemistry for DPPIV was carried out. DPPIV enzyme activity was detected as previously described.[15] $DPPIV^+$ foci in livers were photographed using a microscope equipped with a CCD camera, and the area of each focus was measured using ImageJ software (http://rsb.info.nih.gov/ij/index.html).

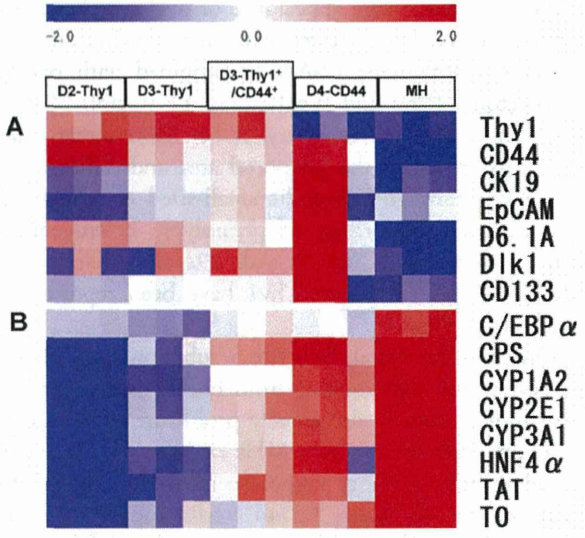

Fig. 1. Gene expression of sorted GalN-D2-$Thy1^+$ cells, D3-$Thy1^+$ cells, D3- $Thy1^+/CD44^+$ cells, and D4-$CD44^+$ cells. The gene-expression pattern of sorted cells was analyzed using GeneChip (Affymetrix, Inc., Santa Clara, CA). MHs isolated from a healthy adult rat liver were used as a control. A heatmap for genes that are classified into (A) stem cell and HPC markers and (B) hepatic markers. Relative expression of genes is shown in $\log_2$ scale. Increases in mRNA level are represented as shades of red and decreases as shades of blue.

Statistical Analysis. All data were analyzed using Turkey-Kramer's multiple comparison test. Level of statistical significance was $P < 0.05$. Experimental results are expressed as the geometric mean ± standard deviation.

Results

Characterization of Isolated Cells From Livers Treated by GalN. As previously reported,[15] $Thy1^+$ cells differentiated into hepatocytes through a $CD44^+$ intermediate state, as shown with clonally cultured $Thy1^+$ cells and cell transplantation. This transition likely happened in the GalN-treated rat liver as well. GeneChip data (Affymetrix, Inc., Santa Clara, CA) indicated that the immature hepatocyte markers, Dlk[21] and AFP were up-regulated in $Thy1^+CD44^+$ and $Thy1^-CD44^+$ cells, whereas markers related to hepatic differentiation were gradually up-regulated during the transition from Thy1-D2 to CD44-D4 cells (Fig. 1). The results also suggested that most D2-$Thy1^+$ cells were not committed to the hepatic lineage. This is consistent with our previous finding that $Thy1^+$ cells isolated from GalN-D2 could form a few epithelial cell colonies in the standard medium for SH induction, whereas those from GalN-D3 certainly formed colonies consisting of $CD44^+$ cells. Therefore, we

Table 1. Effects of Growth Factors and Cytokines on the Formation of Epithelial Cell Colonies

Growth Factors	Numbers of Colonies/Well	Numbers of Cells/Colony
Control	0	0
EGF	4.5 ± 3.8	41.4 ± 1.8
bFGF	0.3 ± 0.6	13.0 ± 0.0
HGF	1.0 ± 1.7	24.6 ± 11.7
LIF	0	0
TNF-α	0	0
IFN-γ	0	0
OSM	0	0
PDGF-BB	0	0
SCF	0	0
IL-6	0	0
TGF-β1	0	0
TGF-β2	0	0

Abbreviations: LIF, leukemia inhibitory factor; OSM, oncostatin M; PDGF-BB, plate-let-derived growth factor BB; SCF, stem cell factor.

considered the possibility that Thy1$^+$ cells became the hepatocyte lineage between D2 and D3. To specify the factors that trigger hepatic commitment, we compared expression patterns of genes related to receptors of growth factors and cytokines and selected 12 candidates (Table 1).

Induction of Epithelial Cell Colonies by Growth Factors. D2-Thy1$^+$ cells were cultured in the medium supplemented with each factor. To elucidate the formation of epithelial cell colonies, ICC for CD44 was conducted 10 days after plating. Of the 12 candidates, only epidermal growth factor (EGF), basic fibroblast growth factor (bFGF), and hepatocyte growth factor (HGF) could induce colonies (Fig. 2A; Table 1). CD44 expression of cells varied among the colonies, and some colonies consisted of cells with low expression of CD44 (CD44$^-$ cells). Next, we examined whether bFGF and/or HGF could enhance the formation and expansion of colonies in the culture with EGF (Fig. 2B). Compared to EGF only (control), the addition of bFGF or HGF did not enhance the frequency of colony formation. In the combination of EGF and bFGF or HGF, the number of cells per colony increased to twice as many as in the control (Fig. 2C). In addition, the combination of the three factors also dose dependently increased the number of cells per colony. These results suggested that a certain number of Thy1$^+$ cells possessed the ability to differentiate into hepatic cells, and that the induction was initiated by EGF, bFGF, and/or HGF.

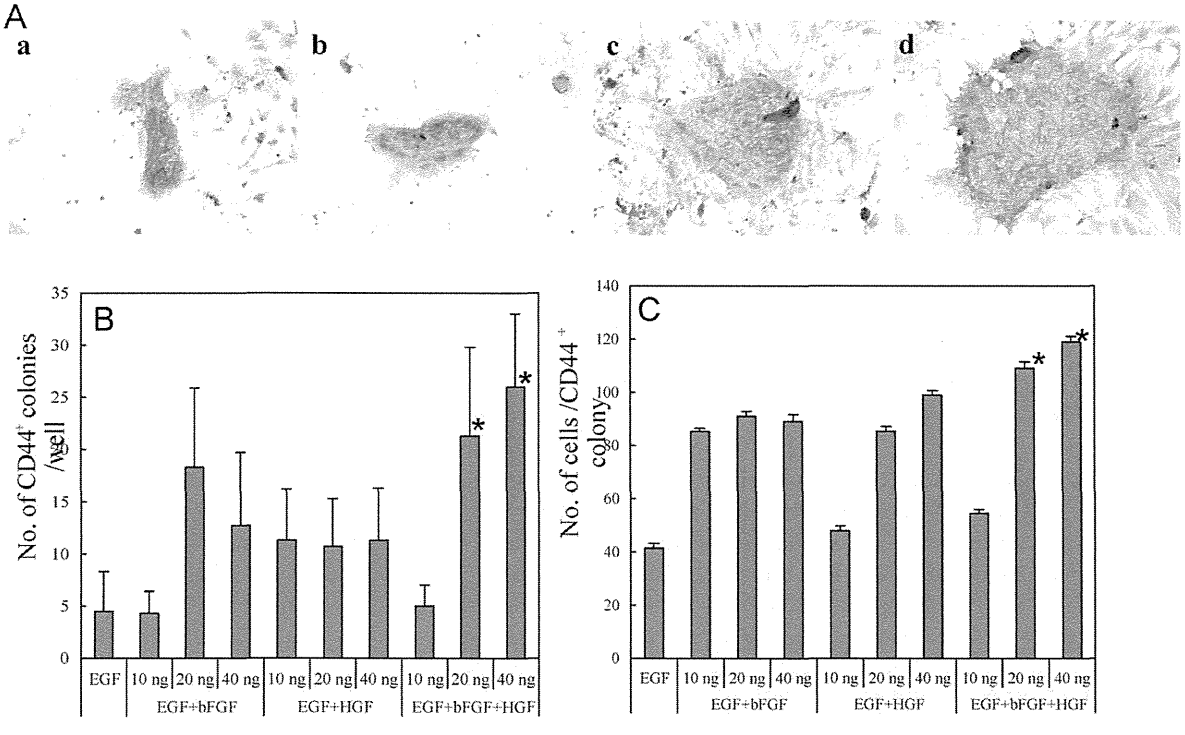

Fig. 2. Induction of CD44-positive cell colonies from sorted D2-Thy1$^+$ cells by treatment with EGF, bFGF, and/or HGF. Thy1$^+$ cells (1×10^5 viable cells/well) sorted from the GalN-D2 liver were plated on 12-well plates and cultured in medium supplemented with EGF (a), EGF+bFGF (b), EGF+HGF (c), and EGF+bFGF+HGF (d) for 10 days. Dose dependency of colony formation was examined. To identify colonies, ICC for CD44 was carried out. The number of CD44$^+$ cell colonies per well (B) and that of cells per colony (C) were measured. Asterisks shown in (B) and (C) indicate significance: $P < 0.05$, compared to EGF and 10 ng of EGF+bFGF+HGF.

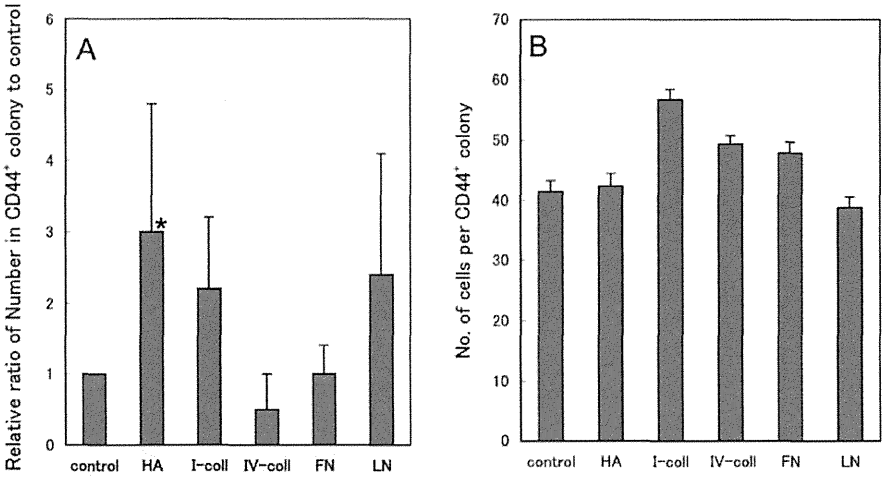

Fig. 3. Effects of ECM on colony formation of Thy1$^+$ cells were investigated. Thy1$^+$ cells were isolated from GalN-D2 rat livers and plated on dishes coated with hyaluronic acid (HA), type I collagen (I-coll), type IV collagen (IV-coll), fibronectin (FN), and laminin (LN). Noncoated dishes were used as controls. Cells were cultured in medium with EGF. To identify the colony, ICC for CD44 was carried out. The number of CD44$^+$ cell colonies per dish (A) and that of cells per colony (B) were measured. Asterisk shows significance: $P < 0.05$, control versus HA.

Induction of Epithelial Cell Colonies by Extracellular Matrix. Because CD44 is one of the receptors of hyaluronic acid (HA)[22,23] and because SHs can selectively proliferate on HA,[18] we investigated whether extracellular matrix (ECM) affected the frequency of emergence and phenotype of colonies derived from D2-Thy1$^+$ cells. Sorted D2-Thy1$^+$ cells were cultured on dishes coated with type I collagen, fibronectin, laminin, and HA, and ICC for CD44 was performed 10 days after plating. When cells were cultured in the medium supplemented with EGF, frequency of colony formation was significantly higher for cells on HA-coated dishes than for the control (Fig. 3A), but no difference was observed in the number of cells per colony among the dishes with each ECM (Fig. 3B).

Growth Ability and CD44 Expression of Cells Sorted From GalN-D3. Thy1$^+$CD44$^-$ (Thy1), Thy1$^+$CD44$^+$, and Thy1$^-$CD44$^+$ (CD44) cells sorted from a GalN-D3 liver were cultured in the medium with EGF for 10 days. Double ICC for CD44 and BrdU was carried out (Fig. 4A–C). The frequency of colony formation was more than four times higher for CD44 cells than for both Thy1 and Thy1$^+$CD44$^+$ cells (Fig. 4D), and the average number of cells per colony was significantly larger for CD44 cells than for Thy1 and Thy1$^+$CD44$^+$ cells (Fig. 4E). The percentages of BrdU$^+$ cells were approximately 70% and 80% in colonies derived from Thy1 and CD44 cells, respectively (Fig. 4A–C, F). Growth ability of Thy1$^+$CD44$^+$ cells was also intermediate between those of Thy1 and CD44 cells.

Intensity and the localization of CD44 varied among cells forming colonies. In spite of the origin of sorted cells, CD44 protein was usually expressed in cell membranes between cells (Fig. 4C). Some colonies consisted of cells with CD44 protein localized in both the cell membrane and cytoplasm (Fig. 4A, B). The latter type of colony was often observed in the culture of Thy1 cells. CD44 positivity of Thy1$^+$ cells in a colony was approximately 65% at day 5 and increased to approximately 80% at day 10 (Fig. 4G).

Next, to examine whether acquisition of CD44 expression in Thy1$^+$ cells was also correlated to growth ability of cells *in vivo*, cell transplantation was carried out. D2-Thy1$^+$, D3-Thy1$^+$CD44$^-$, D3-Thy1$^+$CD44$^+$, D3-Thy1$^-$CD44$^+$, and D4-CD44$^+$ cells (5×10^5 cells/rat) isolated from GalN-treated livers were intrasplenically transplanted into RET/PH-treated rats. One month after transplantation, the number of cells in foci derived from D4-CD44 was much larger than in those from Thy1-expressing cells (Fig. 4H, I). The growth rate of engrafted cells increased in correlation with the expression of CD44 and time after GalN treatment. In addition, no types of donor-derived (Y chromosome$^+$) cells, other than hepatocytes, could be found in recipient livers (Supporting Fig. 1).

Gene Expression of Hepatic Markers of Epithelial Cell Colonies Derived From D3-Thy1 Cells. To elucidate the characteristics of cells in colonies derived from D3-Thy1 cells, quantitative polymerase chain reaction (qPCR) of cells was performed for each colony, which was separated from the culture dish using a